SWITCHED-BEAM ANTENNA FOR WIRELESS SENSOR NETWORK NODES

Luca Catarinucci[*], Sergio Guglielmi, Luigi Patrono, and Luciano Tarricone

Department of Innovation Engineering, University of Salento Via per Monteroni, Lecce 73100, Italy

Abstract—Directional and switched-beam antennas in wireless sensor networks are becoming increasingly appealing due to the possibility to reduce transmission power and consequently extend sensor node lifetime. In this work, a reconfigurable beam-steering antenna is proposed for Wireless Sensor Network applications in the ISM band ($f = 2.4$–2.4835 GHz). The proposed radiating structure consists of a vertical half-wavelength dipole antenna and eight microstrip antennas composed of a rectangular two-element patch antenna array. These microstrip antennas have a directional radiation pattern in the azimuth plane with a HPBW of nearly 60 degrees. A control circuit consisting of a transmission line, RF-switches and a 4 : 16 multiplexer has been designed in order to dynamically switch among nine radiation patterns, eight directional and one omnidirectional. Simulations and experimental results, referred to a low-cost realization on a FR4 substrate with a thickness of 1.6 mm, demonstrate appreciable performance.

1. INTRODUCTION

Wireless sensor networks consist of small, low-power and energy-constrained sensor nodes placed over an area of interest in order to monitor physical or environmental conditions and to deliver sensory data to collection point. Each node has a limited memory to store data and program code, a CPU for local processing, a set of transducers to acquire information about the surrounding environment, a wireless communication system for data transmission, usually equipped with an omnidirectional antenna, and a battery that supplies the energy needed by the device to perform programmed tasks.

* Corresponding author: Luca Catarinucci (luca.catarinucci@unisalento.it).

One of the most important issues in WSN contexts is the energy saving. Working in hardly accessible or unpractical places, it could be impossible or inconvenient to replace batteries; hence the lifetime of a WSN node should be long enough to perform all the required application tasks and in some cases it must be long several months, or even years.

Many studies have shown that wireless data transmission is the most expensive operation in terms of energy consumption [1–3]; the energy cost to transmit a single bit is approximately the same needed to process thousand operations in node's CPU. Hence most of the techniques proposed in the literature to minimize the energy consumption use protocols that reduce data transmission or switch off radio transceiver, turning the node into a sleep mode. However, in some scenarios, these techniques may reduce network performance or may not be sufficiently reactive to network changes.

Some other solutions propose the use of fully-passive WSN nodes based on Radiofrequency Identification (RFID) [4–7], where the RFID readers energize and interrogate the nodes. Despite the system has been successively validated [8], it is not compliant with WSN standards.

Another way to reduce energy consumption and extend sensor operation time is to use directional or switched-beam antennas. Traditionally, WSN nodes are equipped with an omnidirectional antenna; in such a case, most of the transmitted power is wasted, just because the power is not focused towards the proper direction, but is equally radiated in all directions.

The rapid development of radio communications and fabrication techniques together with the use of higher and higher frequencies has favored the antennas miniaturization. This has led to an increasing number of studies on the beam-steering antennas and their applications in different fields of radio technologies. Nevertheless, the integration of beam-steering antennas in WSNs to reduce energy consumption and to extend sensor nodes lifetime, has not been exhaustively explored yet.

In particular, an interesting switched-beam directional antenna is proposed in [9]. It is composed of four planar patch antennas arranged in a box-like structure. Such an antenna system ensures a uniform coverage of the whole horizon plane when switching between the antennas. Nevertheless, a single almost uniform radiation pattern, crucial in the addressed context, cannot be obtained.

The pattern reconfigurable antenna for WSN sink nodes presented in [10] is rather interesting as well. It can switch between conical to front-directional pattern and vice versa. Even though it shows a remarkable peak gain in front directional beam patterns, it is rather

cumbersome and, moreover, does not allow an omnidirectional pattern.

On the contrary, a rather compact Switched-Beam Antenna is presented in [11]. It is composed of a four-element antenna array and shows eight directional patterns and an omnidirectional one, ensuring an uniform coverage of the 360 degree horizon. It has a compact size and low manufacture cost, but exhibits a HPBW of nearly 120 degrees which causes a large overlapping area of beams, thus not ensuring an optimized energy saving.

A reconfigurable angular diversity antenna, constructed with quad corner reflector arrays and a switching control is proposed in [12]. It shows a high radiation gain, but occupies a large volume.

A pattern reconfigurable antenna was proposed in [13]. It is a microstrip parasitic array antenna with a small size and a simple structure but it does not ensure a coverage of 360 degrees in the azimuth plane.

Vice versa, in this work a reconfigurable beam-steering antenna for WSN applications in the ISM band is proposed. It can be connected to the wireless module of a sensor node and work in place of the common omnidirectional antenna. It consists of a vertical half-wavelength dipole antenna and eight microstrip antennas with a directional radiation pattern in the azimuth plane. Thanks to a control circuit consisting of a transmission line, RF-switches and a multiplexer, it is possible to dynamically switch among the nine radiation patterns (eight directional and one omnidirectional).

The paper is structured as follows: in Section 2 the working principle and the design of proposed antenna are described; later on in in Section 3 simulated and experimental results are shown and discussed; finally, conclusions are reported in Section 4.

2. SWITCHED-BEAM ANTENNA DESIGN

This section focuses on the working principle and architecture of the proposed reconfigurable beam-steering antenna in the ISM band ($f = 2.4$–$2.4835\,\text{GHz}$).

The idea is to realize a radiating structure allowing the selection of a specific radiation pattern among nine possibilities. More specifically, one of them should radiate omnidirectionally, the other eight ones should illuminate a specific direction that is $n * \pi/4$ in the azimuth plane, where $n = 0, \ldots, 7$. An overlapping of almost 15 degrees should be guaranteed. Moreover, the radiation pattern selection should be controlled through a specific digital interface. In this way, it will possible to cover 360 degrees in the horizontal plane, with adjacent patterns spaced 45 degrees.

The proposed switched-beam antenna consists of eight identical directional microstrip array antennas each one providing a radiation pattern with a HPBW of nearly 60 degrees and a gain of nearly 7 dBi in the main lobe direction, and a vertical half-wavelength dipole antenna with an omnidirectional pattern. The radiating antenna is dynamically selected through a specific control circuit so as to conform the radiation patterns accordingly.

The proposed radiating structure can be connected to a generic electronic device provided by an U.FL connector (an ultra-small surface mount coaxial connector for high-frequency signals) for the RF signal and an output interface with at least 4 digital pins (e.g., General Purpose Input/Output interface) in order to control the switching circuit.

In order to better understand the practical operation of the proposed antenna, a block diagram of the switching process has been depicted in Figure 1. The RF input signal is directed to one of the nine outputs of the switching system by setting specific combinations of bits on the 4-pin interface. Nine combinations of bits have been set, each corresponding to a specific output connected to a radiating element.
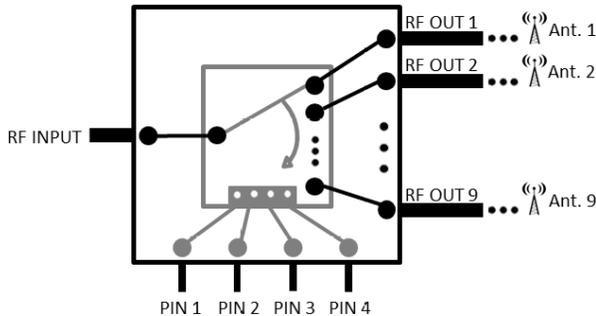
Figure 1. Block diagram of the switching circuit.

Specific details about switching circuit and radiating elements will be provided in Sections 2.1 and 2.2 of this chapter.

2.1. RF Switching Circuit

The structure of the proposed RF switching circuit is depicted in Figure 2, whilst the whole circuit layout is given in Figure 3(a). Basically, the switching circuit is composed of nine RF-switches placed on the terminations of a microstrip transmission line in star
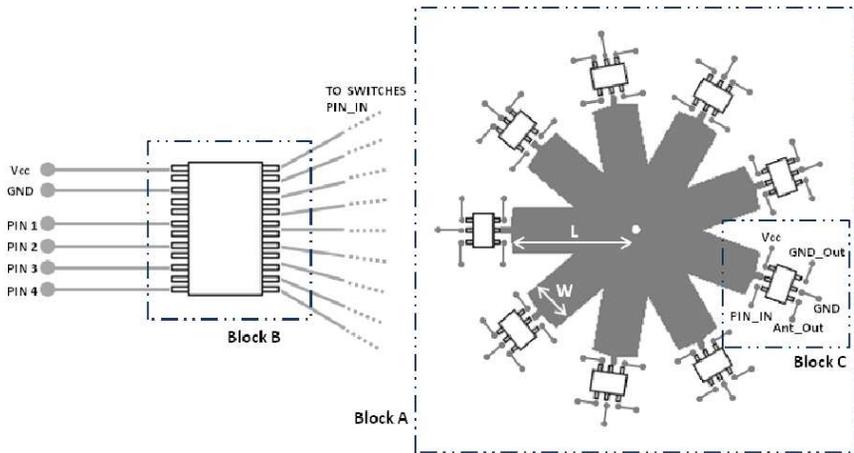
Figure 2. Structure of proposed RF switching circuit.

configuration and a multiplexer with four digital inputs used to control the entire circuit. The transmission line is fed through a $50\,\Omega$ U.FL connector at its center point.

Block A of Figure 2 shows the RF transmission line in star configuration composed of nine quarter-wavelength-long branches. Actually, due to the presence of the switches at the branches terminations, it has been necessary to reduce the physical length L of each line. In particular, during simulation and optimization phases, the switches have been modelled with an equivalent circuit composed of a capacitance and a resistance in series, according to the datasheet of the used devices. The result of such an optimization phase is $L = 0.18\lambda$.

Moreover, as described in [14], using a FR4 substrate with dielectric constant $\varepsilon = 37$ @ $2.45\,\text{GHz}$ and thickness $h = 1.6\,\text{mm}$, a transmission line with width W of $3.3\,\text{mm}$ has been obtained:

$$W = d\left\{\frac{2}{\pi}\left[B - 1 - \ln\left(2B - 1\right)\right] + \frac{\varepsilon_r - 1}{2\varepsilon_r}\left[\ln\left(B - 1\right) + 0.39 - \frac{0.61}{\varepsilon_r}\right]\right\}$$

$$A = \frac{Z_0}{60}\sqrt{\frac{\varepsilon_r + 1}{2}} + \frac{\varepsilon_r - 1}{\varepsilon_r + 1}\left(0.23 + \frac{0.11}{\varepsilon_r}\right); \quad B = \frac{377\varepsilon}{2Z_0\sqrt{\varepsilon_r}}$$

$$d = 1.6\,\text{mm}; \quad \varepsilon_r = 3.9; \quad Z_0 = 50\,\Omega; \quad W \approx 3.25\,\text{mm} \Rightarrow W \approx 3.3\,\text{mm};$$

The switching circuit basic operation is to dynamically connect a branch of the line to an antenna element with $50\,\Omega$ input impedance (as described below, a directive antenna resonant at $2.45\,\text{GHz}$ frequency) and terminate remaining branches in a short-circuit, through nine RF switches.
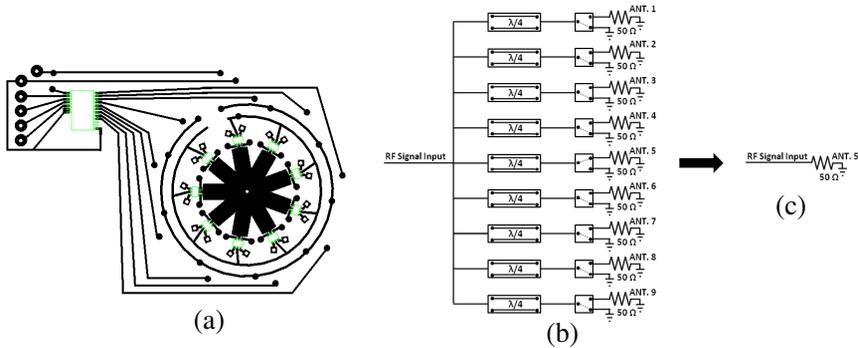
Figure 3. (a) Layout of the switching circuit, (b) schematic of the proposed antenna system in one of the possible switching configuration and (c) its equivalent.

According to transmission line theory [15], each branch of the transmission line works like a quarter-wave impedance transformer that presents at its input the dual impedance seen on the line termination. For this reason, a short-circuited branch exhibits at its input a theoretically infinite impedance likewise an open circuit.

As shown in Figure 3, the designed structure presents at any time one of the branches connected to an antenna element and all the remaining branches short-circuited. In this way, the RF input port sees always eight open lines, corresponding to the eight short-circuited lines, and a $50\,\Omega$ terminated line, corresponding to the selected antenna element.

As shown in Block B of Figure 2, the multiplexer used for the control circuit is a 4–16 analog multiplexer with four binary weighted address inputs (*PIN 1,...,4*); only nine outputs have been used to control the *PIN IN* control input of the switches, through nine combinations of the four input bits. It is powered with a 3.3 V supply through the input pins *VCC* and *GND*.

The switches in Block C of Figure 2 used to select the different antenna elements are SPDT RF-switches with a pin for the RF input signal, two for the RF output signal (*Ant_Out and GND_Out*), a logic control input (*PIN_IN*) and two for the power supply (*VCC* and *GND*).

According to the control signal input, these devices dynamically connect the transmission line with the *Ant_Out* or *GND_Out* outputs. As for the multiplexer, the switches are powered by 3.3 V supply through the lines *VCC* and *GND*.
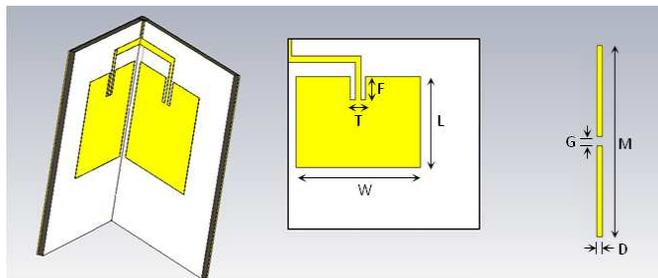
Figure 4. Geometry of the directive antenna element and half-wavelength dipole. $W = 3.55 \, \text{mm}$, $L = 28.3$, $F = 7.4 \, \text{mm}$, $T = 5 \, \text{mm}$, $D = 0.244 \, \text{mm}$, $M = 59.225$, $G = 0.306 \, \text{mm}$.

2.2. Antenna Element (Rectangular Two-element Patch Antenna Array)

As previously stated, the proposed radiating structure consists of a vertical half-wavelength dipole antenna and eight identical microstrip antennas with a directional pattern.

As for the dipole, represented in Figure 4, a simple copper-made wire (width 0.306 mm and length 59 mm) has been used.

Vice versa, as for the directive antenna elements, in order to obtain a radiation pattern in the azimuth plane with a HPBW of nearly 60 degrees without strongly impacting upon the antenna dimension, each element has been designed as an array of two rectangular patch antennas in a 3D configuration, as shown in the same Figure 4.

As well known, a generic microstrip antenna consists of a dielectric substrate between a ground-plane and a radiating rectangular patch in a planar configuration. The length (L) and the width (W) of the rectangular patch determine the antenna radiation resistance and its operating frequency [16]. Usually a single square patch microstrip antenna have a length (L) equal to $\lambda/2$, a linear polarization and a HPBW of nearly 180 degrees.

The simplest approach in order to reduce the HPBW parameter consists in designing a n-element planar patch array, studying the coupling between the antenna elements as a function of the mutual position of the elements. This approach, however, causes a considerable increase of the structure dimensions. Another approach is to design a corner reflector antenna with a half-wavelength dipole placed on the bisector of the corner angle of a conducting surface bent at an angle of less than 90 degrees. However, as the angle gets smaller, the antenna tends to get larger and the dipole feed impedance becomes lower.

The proposed directive antenna combines the qualities of these

(a)   (b)
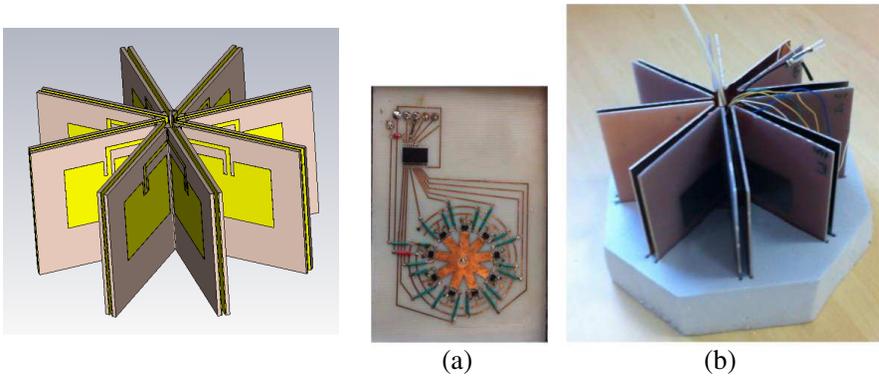
Figure 5. Geometry of   **Figure 6.** (a) Realized switching circuit
the proposed antenna.   and (b) switched-beam antenna.

approaches, in order to reduce the structure dimension; it is designed
as a simple rectangular, two-element patch antenna array [17] bent at a
45 degrees angle on the middle of the structure. As shown in Figure 5,
this 3D configuration allows a positioning of eight identical antennas
in a circular compact structure that significantly reduces the size of
entire antenna. This structure ensures a uniform coverage of the 360
degrees horizon through the eight radiation patterns in the azimuth
plane with a HPBW of nearly 60 degrees.

The entire RF structure has been modeled with the full-
wave simulator CST-MS (Computer Simulation Technology-Microwave
Studio). Return loss and radiation properties have been calculated
by modeling the RF switches by means of proper equivalent circuits
according to the datasheet.

In order to verify proper operation and performance of the
proposed switched-beam antenna, a prototype has been realized on
a FR4 substrate ($\varepsilon = 3.7$ @ 1 GHz, $h = 1.6$ mm).

The used multiplexer is a Philips 74HC/HCT4514 4-to-16 line
decoder/demultiplexer having four binary weighted address inputs,
with latches, a latch enable input, an active low enable input and
16 outputs that are mutually exclusive. It is characterized by a
propagation delay equal to 23 ns, an input capacitance equal to 3.5 pF
and an input maximum voltage equal to 6 V. The used switches are
Peregrin PE4283 RF UltraCMOS switches with a single-pin CMOS
logic control input, a 1.5 kV ESD tolerance, a low insertion loss of
0.65 dB at the reference frequency, an isolation of 33.5 dB between the
output ports, a switching time of 0.65 μs, a +3 V power supply input
and a operation band ranging from DC to 4 GHz.

A picture of both the switching circuit and one of the realized switched-beam antennas are given in Figure 6. The overall size of the antenna is 15 cm in diameter and 7 cm in height.

3. VALIDATION RESULT

Several tests and measures have been performed in order to obtain an accurate characterization of the electromagnetic properties of the proposed antenna; for this purpose, an Agilent 3444/7 VNA (Vector Network Analizer) has been used. Furthermore, as will be explained below, a study of the radiation patterns has been performed through the use of STM32W-EXT WSN boards with a 32 bit ARM microprocessor and a IEEE 802.15.4-compliant transceiver.

Figure 7 shows the measured return loss of the RF switching circuit transmission line in the case of connection with a 50 Ω load. The circuit shows good impedance matching in the highlighted ISM band (2.4–2.4835 GHz) with return loss better than 20 dB.
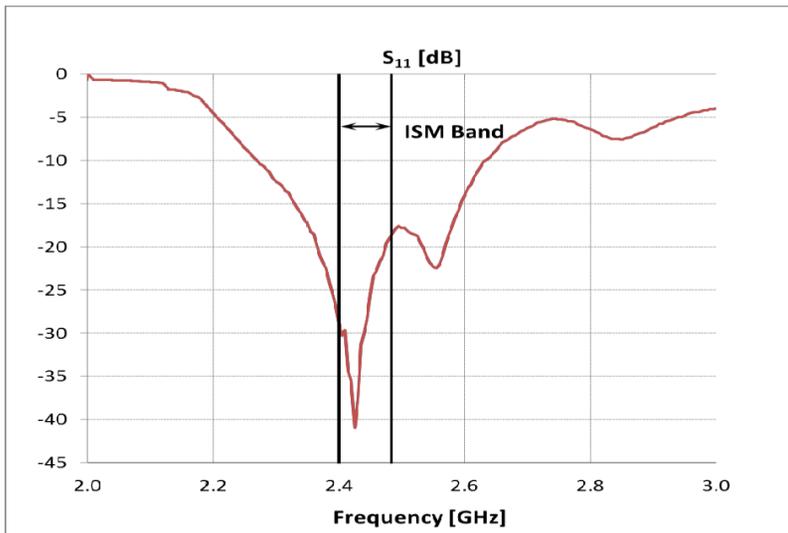
Figure 7. Measured return loss of the RF switching circuit transmission line in the case of connection with a 50 Ω load.

Figure 8 shows the S_{21} scattering parameter measured on the terminations of a branch of the transmission line, more precisely between the RF signal input port and *Ant_Out* pin of the switch (see block C of Figure 2). Results related to the two possible switch
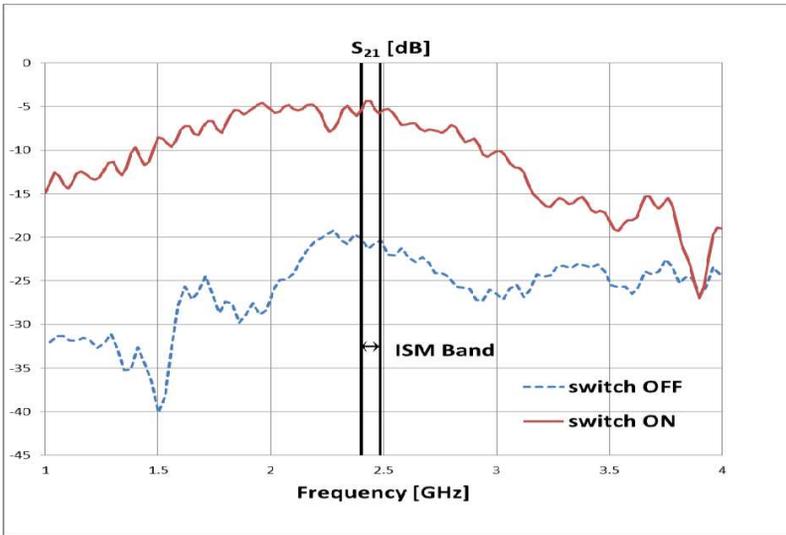
Figure 8. Measured S_{21} scattering parameter of the RF switching circuit in the case of direct connection between RF input port and *Ant_Out* pin (switch ON), and between RF input port and *GND_Out* pin (switch OFF). Continuous curve is referred to the switch ON case, whilst dotted curve to the switch OFF case.

configurations are reported: switch ON in the case of direct connection between transmission line and *Ant_Out* pin and switch OFF in the case of direct connection between transmission line and *GND_Out* pin. Such results show a signal attenuation of less than 4 dB when the switch connects a branch of the transmission line with the antenna element output, and a signal attenuation of more than 20 dB when the switch connects a branch of the transmission line with the ground plane. So the proper operation of the switching circuit is demonstrated; indeed, the very high measured attenuation in the case of switch OFF ensures that one and only one antenna element will transmit, at any time.

The measured return loss compared with the simulated results for the single directive antenna element are reported in Figure 9. The directive antenna element shows good impedance matching with an observed return loss better than 25 dB.
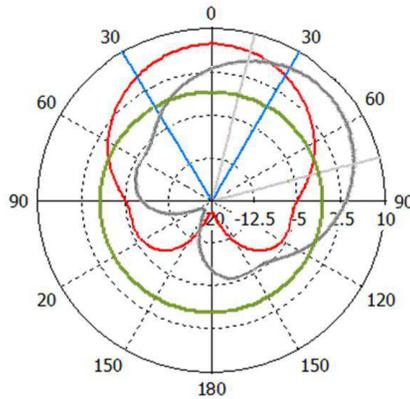
The simulated radiation patterns for the vertically polarized directive antenna element have also been computed and are reported in Figure 10(a) for the azimuth plane ($\varphi = 0°$) and in Figure 10(b) for the elevation plane ($\varphi = 90°$). The computed main lobe magnitude is 7.2 dBi, the side lobe level is −9 dB and the cross-polarization level
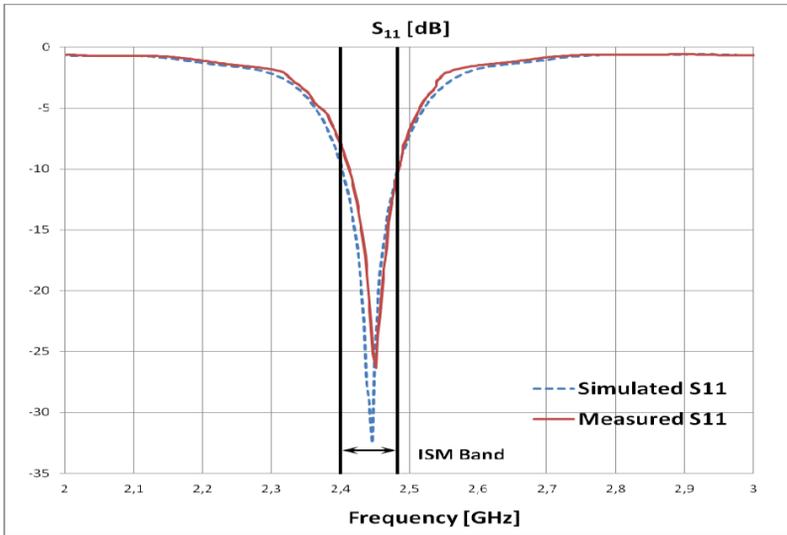
Figure 9. Measured and simulated return loss of the single directive antenna element.
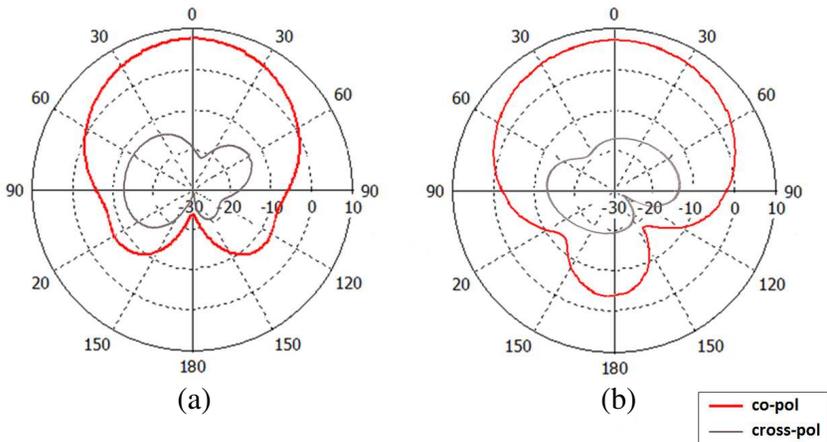
Figure 10. Simulated radiation patterns for the vertically polarized directive antenna element (a) for the azimuth plane and (b) for the elevation plane.

Figure 11. Simulated radiation patterns of two successive directive antennas and of the half-wavelength dipole in the azimuth plane.

is -21 dB. Moreover the Half power beam width (HPBW) is nearly 60 degrees for the azimuth plane according to the proposed design specifications.

A representation of directional beams of two consecutive directive antennas and of the omnidirectional half-wavelength dipole one is reported in Figure 11. Moreover the HPBW of each beam is reported in order to demonstrate the proper functioning of the proposed switched-beam antenna, in terms of overlapping area and beam width.

As further validation, as previously mentioned, in order to accurately characterize the radiation properties of the proposed antenna, several tests with WSN nodes operating in the ISM band have been performed. In particular, two STM32W108B-KEXT devices have been used, one connected to the proposed antenna and statically positioned in the middle of a 40 square meters area, and the other, with a standard omnidirectional configuration, used to measure the number of packets received in different points of the same area. For each radiator, the diagram individuating the portion of the area where more than 95% of the sent packets is correctly received corresponds to the related actually covered area.

As shown in Figure 12 the measurement points are disposed on concentric circumferences with a minimum radius of 4 m (R_1) and a maximum radius of 18 m (R_n) with an angular distance of $10°$. In particular, Figure 12(a) shows the obtained diagrams for two adjacent directive radiators (red and grey curves) as well as for the half-wavelength dipole one (green curve); black dots represent measurements points (see Figure 12(b) for the experimental setup).
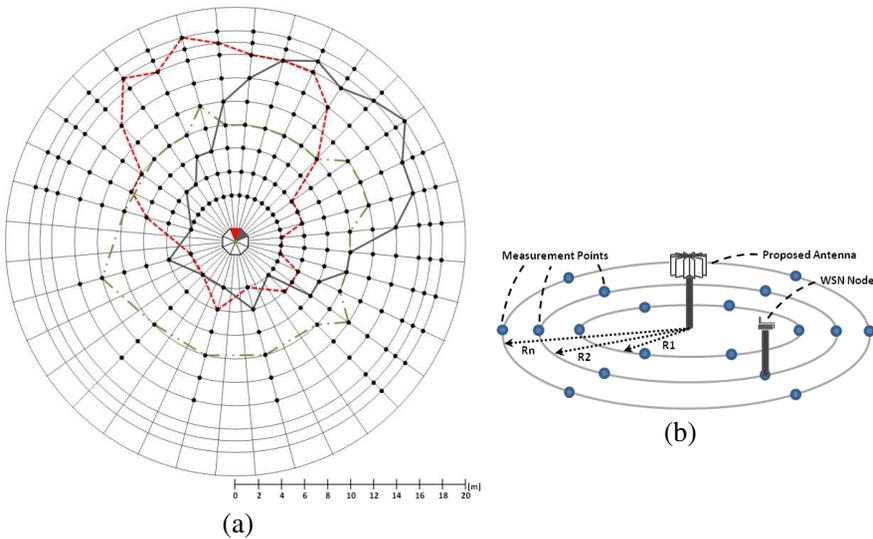
Figure 12. Diagrams representing the regions where a real WSN node correctly receive more than 96% of packets for three different radiators: (a) 2 adjacent directive radiators and the half-wavelength dipole and (b) related experimental setup.

In each case, the same emitted power has been considered.

As expected, it can be observed the proper functioning of the proposed switched-been antenna. Indeed, directive elements guarantee longer working range than the half-wavelength dipole, which is, as expected, substantially omnidirectional in the azimuth plane. Alternatively, a lower power could be radiated to guarantee the same working distance.

Moreover, as desired, coverage areas associated to adjacent directive antennas guarantee a suitable overlapping area and a beam width compatible with the simulated one. In fact, despite conceptually different, the behaviour of the radiation patterns of Figure 11 can be compared with those of the diagrams of Figure 12. A substantial agreement can be observed for both directive radiators and half-wavelength dipole.

4. CONCLUSIONS

In this work a switched-beam antenna particularly suitable for WSN applications has been presented. It is composed of eight directional radiators and an omnidirectional one. The most appropriate radiator is selected according to the context-dependent needs of the WSN by

means of a properly designed control circuit. Each directional radiator is a two-element patch antenna array, whilst a simple half-wavelength dipole has been used for the omnidirectionality in the horizontal plane. As for the control circuit, it is composed of nine RF-switches, a transmission line in star configuration, and a 4 : 16 multiplexer. The device has been extensively tested, and obtained results demonstrate the appropriateness of the proposed approach.

REFERENCES

1. Anastasi, G., M. Conti, M. Francesco, and A. Passarella, "Energy conservation in wireless sensor networks: A survey," *Ad Hoc Networks*, Vol. 7, No. 3, 537–568, 2009.

2. Girban, G. and M. Popa, "A glance on WSN lifetime and relevant factors for energy consumption," *Computational Cybernetics and Technical Informatics (ICCC-CONTI)*, 2010.

3. Chen, Y. and Q. Zhao, "On the lifetime of wireless sensor networks," *IEEE Communications Letters*, Vol. 9, No. 11, 2005.

4. Catarinucci, L., R. Colella, and L. Tarricone, "A cost-effective UHF RFID tag for transmission of generic sensor data in wireless sensor networks," *IEEE Transactions on Microwave Theory and Techniques*, Vol. 57, No. 5, Part 2, 1291–296, 2009.

5. Catarinucci, L., R. Colella, and L. Tarricone, "A new enhanced UHF RFID sensor-tag," *Proc. of the 5th European Conference on Antennas and Propagation, EUCAP 2011*, Rome, Italy, Apr. 2011.

6. Catarinucci, L., R. Colella, and L. Tarricone, "Optimized antennas for enhanced RFID sensor tags," *Proc. of IEEE Antennas and Propagation Society, AP-S International Symposium (Digest)*, Spokane, Washington, Jul. 2011.

7. Catarinucci, L., R. Colella, and L. Tarricone, "Enhanced UHF RFID sensor-tag," *IEEE Microwave and Wireless Components Letters*, Vol. 23, No. 1, 49–51, Jan. 2013.

8. Catarinucci, L., R. Colella, A. Esposito, L. Tarricone, and M. Zappatore, "RFID sensor-tags feeding a context-aware rule-based healthcare monitoring system," *Journal of Medical Systems (JOMS)*, Vol. 36, No. 6, 3435–3449, Springer, 2011.

9. Giorgetti, G., A. Cidronali, S. K. S. Gupta, and G. Manes, "Exploiting low-cost directional antennas in 2.4 GHz IEEE 802.15.4 wireless sensor networks," *Proceedings of the 10th European Conference on Wireless Technology*, 2007.

10. Lai, M.-I., T.-Y. Wu, J.-C. Hsieh, C.-H. Wang, and S.-K. Jeng,

"Pattern reconfigurable antenna for a wireless sensor network sink node," *Microwave Conference Proceedings (APMC)*, 2010.

11. Lai, M.-I., T. Y. Wu, J. C. Hsieh, C. H. Wang, and S. K. Jeng, "Compact switched-beam antenna employing a four-element slot antenna array for digital home applications," *IEEE Transactions on Antennas and Propagation*, Vol. 56, No. 9, 2929–2936, 2008.

12. Chang, D.-C., B.-H. Zeng, and J.-C. Liu, "Reconfigurable angular diversity antenna with quad corner reflector arrays for 2.4 GHz applications," *IET Microwaves, Antennas & Propagation*, Vol. 3, No. 3, 522–528, 2009.

13. Zhang, S., G. H. Huff, and J. T. Bernhard, "A pattern reconfigurable microstrip parasitic array," *IEEE Transactions on Antennas and Propagation*, Vol. 52, No. 10, 2773–2776, 2004.

14. Collin, E., *Foundation of Microwave Engineering*, McGraw Hill, New York, 2007.

15. Wadell, B. C., *Transmission Line Design Handbook (Artech House Antennas and Propagation Library)*, Artech House Microwave Library, 1991.

16. Garg, R., P. Bhartia, I. Bahl, and A. Ittipiboon, *Microstrip Antenna Design Handbook (Artech House Antennas and Propagation Library)*, Artech House Microwave Library, 2001.

17. Balanis, C. A., *Antenna Theory: Analysis and Design*, 3rd edition, John Wiley & Sons, 1997.